Imaging Metabolism with Hyperpolarized ^{13}C-Labeled Cell Substrates

Kevin M. Brindle*

Department of Biochemistry, University of Cambridge, Tennis Court Road, Cambridge CB2 1GA, U.K.
Li Ka Shing Centre, Cancer Research UK Cambridge Institute, Robinson Way, Cambridge CB2 0RE, U.K.
CRUK & EPSRC Cancer Imaging Centre in Cambridge and Manchester, U.K.

ABSTRACT: Non-invasive ^{13}C magnetic resonance spectroscopy measurements of the uptake and subsequent metabolism of ^{13}C-labeled substrates is a powerful method for studying metabolic fluxes *in vivo*. However, the technique has been hampered by a lack of sensitivity, which has limited both the spatial and temporal resolution. The introduction of dissolution dynamic nuclear polarization in 2003, which by radically enhancing the nuclear spin polarization of ^{13}C nuclei in solution can increase their sensitivity to detection by more than 10^4-fold, revolutionized the study of metabolism using magnetic resonance, with temporal and spatial resolutions in the seconds and millimeter ranges, respectively. The principal limitation of the technique is the short half-life of the polarization, which at ∼20−30 s *in vivo* limits studies to relatively fast metabolic reactions. Nevertheless, pre-clinical studies with a variety of different substrates have demonstrated the potential of the method to provide new insights into tissue metabolism and have paved the way for the first clinical trial of the technique in prostate cancer. The technique now stands on the threshold of more general clinical translation. I consider here what the clinical applications might be, which are the substrates that most likely will be used, how will we analyze the resulting kinetic data, and how we might further increase the levels of polarization and extend polarization lifetime.

INTRODUCTION

The abundance of tissue water protons and the sensitivity of the proton to NMR detection have allowed imaging of tissue anatomy at relatively high resolution, with image resolutions in pre-clinical studies at high magnetic fields in the 10−100 μm range.[1] Cell metabolites, on the other hand, are present at ∼10 000 times lower concentration than tissue water, and therefore it is not possible to image them at clinical magnetic field strengths, except at relatively low spatial (1 cm^3) and temporal resolutions (5−10 min).[2] Moreover, single ^{1}H spectra, or ^{1}H spectroscopic images of tissue metabolites, provide only a profile of the steady-state metabolite concentrations and lack dynamic information about metabolic fluxes. These can be measured in ^{13}C and ^{1}H spectra by the introduction of isotopically labeled substrates.[3,4] The use of ^{13}C-labeled substrates to investigate metabolic fluxes began in the 1970s with studies in *E. coli* and yeast[5,6] and progressed subsequently to human studies.[3] The technique can be used to follow which metabolites are labeled, and also which positions in these molecules are labeled. The information content can be enhanced by introducing two ^{13}C-labeled substrates and then monitoring multiple labeling of individual cell metabolites through spin−spin coupling of adjacent ^{13}C labels, which can yield information about the relative fluxes through various metabolic pathways.[7] Recent and elegant examples of the application of this approach include studies on glucose, glutamine, and acetate metabolism in tumors.[8,9] Although the sensitivity of ^{13}C label detection can be enhanced by indirect detection via spin-coupled protons,[10,11] this is still not sufficient to enable imaging. The breakthrough for the field came with the demonstration that dissolution dynamic nuclear polarization (dDNP) of ^{13}C-labeled cell substrates can increase their sensitivity to detection by more than 10 000 times.[12] This has made it possible to image not only hyperpolarized ^{13}C-labeled cell substrates, following intravenous injection, but, more importantly, the kinetics of their conversion into cell metabolites, with spatial resolutions of 2−5 mm and temporal resolutions in the sub-second range.[13] The Achilles' heel of the technique, however, is the relatively short half-life of the polarization *in vivo*, which is typically 20−30 s. This limits the number of reactions that can be monitored *in vivo* to those that show fast reaction kinetics. These will usually be catabolic reactions responsible for energy generation rather than the generally slower anabolic reactions involved in cell biosyntheses. The limited lifetime of the polarization also restricts the number of sequential enzyme catalyzed steps through which a ^{13}C label can be followed, although flux of hyperpolarized ^{13}C label from glucose through all 10 steps of the glycolytic pathway to lactate has been detected[14−17] and imaged[18] (Figure 1).

There have been several recent and comprehensive reviews describing the molecules that have been polarized and how they have been used,[19−23] and therefore I do not intend to provide a full coverage of the field. Instead, I will concentrate this Perspective on those substrates that appear to have the greatest potential to be used clinically, or that can be used pre-clinically to address questions of fundamental biological importance that cannot easily be answered using more conventional techniques. The focus is on applications in oncology, which reflects my own research interests.
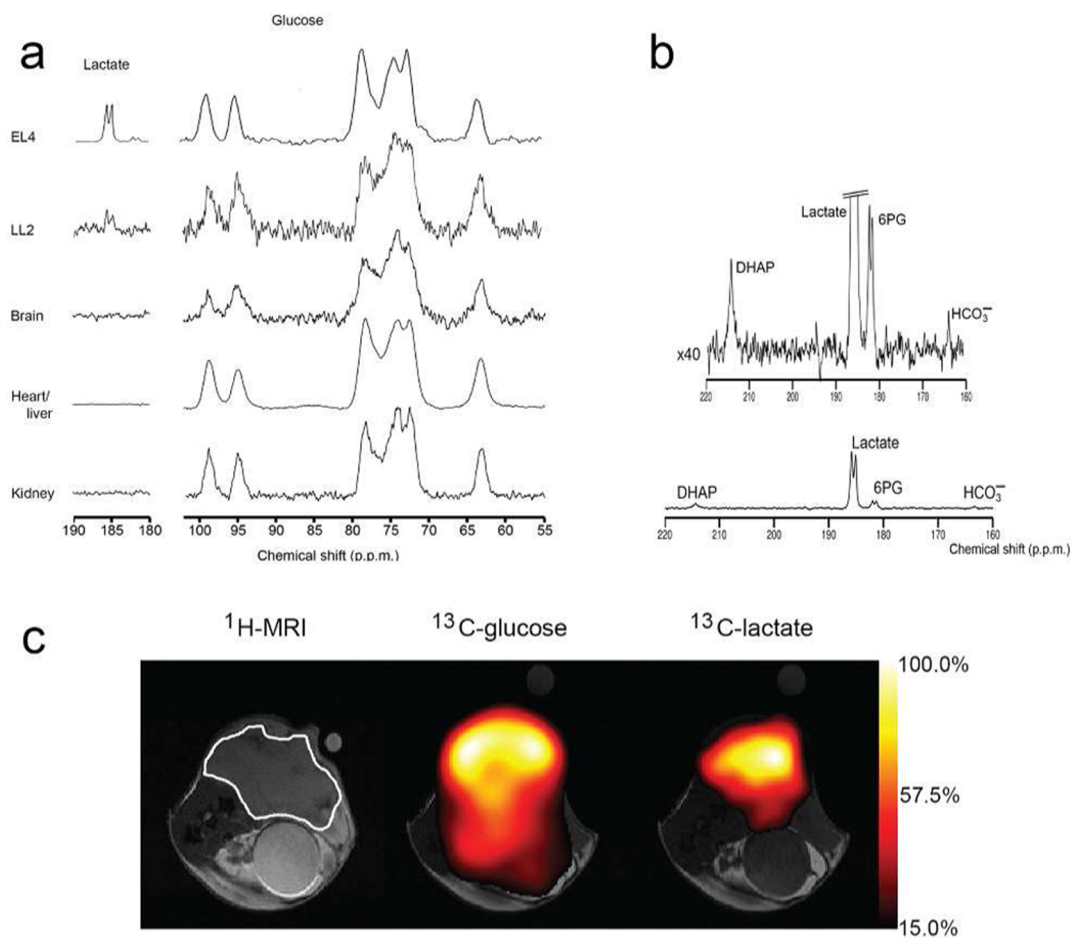
Figure 1. Imaging tumor metabolism with hyperpolarized [U-^{13}C,U-^{2}H]glucose. (a) Localized spectra acquired from the indicated tissues (EL4 and LL2 are implanted tumor models). Only the tumors show signal from labeled lactate. This is not because glycolytic flux is slow in these other tissues, but because, unlike tumors, they do not accumulate lactate under aerobic conditions (i.e., they do not show a "Warburg effect"). (b) Vertical scale expansion of the spectrum between 160 and 220 ppm shows signals from dihydroxyacetone phosphate (DHAP), a glycolytic intermediate, and a signal that is predominantly from 6-phosphogluconate (6PG), an intermediate in the pentose phosphate pathway.[24] (c) There is sufficient signal from the hyperpolarized [U-^{13}C,U-^{2}H]glucose, and the lactate formed from it, to image both metabolites. The lactate signal is concentrated in the tumor, which is visible in the ^{1}H image (outlined in white). Adapted from ref 18 with permission.

■ DYNAMIC NUCLEAR POLARIZATION AND TRANSFER TO THE SOLUTION STATE

Dynamic Nuclear Polarization. The sample to be polarized is mixed with a stable radical, rapidly frozen to form a glass, and then placed in a high magnetic field (typically greater than 3 T) and at low temperature (∼1 K). This low temperature can readily be achieved by boiling-off liquid helium under a vacuum. Crystallization of the sample, which results in the radical concentrating in domains and inhibiting the DNP process, can be prevented by using solvents such as glycerol or dimethyl sulfoxide that promote glass formation. The magnetic moment of the electron is 658 times greater than that of the proton, and at this low temperature and high magnetic field, the electron reaches near unity polarization. The electron spin polarization is then transferred to the nuclear spins by microwave irradiation close to the resonance frequency of the electron spin. Addition of Gd^{3+} ions can be used to shorten the electron spin longitudinal relaxation time, improving the DNP enhancement by 50−100%.[25] Nitroxide and trityl radicals have been used in general, although radicals have also been produced endogenously by UV irradiation of the sample.[26] For transfer of the polarization to be effective, the EPR spectrum of the radical should have a line width that exceeds the Larmor frequency of the nuclear spin. Nitroxides have a broad EPR spectrum, which covers the Larmor frequency of all nuclear spins, whereas trityls have a narrower spectrum and are better for polarizing low gamma nuclei, such as ^{13}C and ^{15}N.[21] There is an optimum radical concentration: while high concentrations shorten the polarization build-up time, they shorten the T_1 of the nuclear spin and lower the steady-state polarization. The build-up time constant can be reduced by using a ^{13}C-labeled glassing agent, which increases the rate of spin diffusion.[27] Spin diffusion is also increased by the high concentration of the ^{13}C-labeled compound to be polarized. Polarization can be improved by increasing the magnetic field strength or by lowering the temperature; however, a drawback is that the polarization build-up times may become very long.[21] An alternative and very promising approach for enhancing the rate of ^{13}C polarization and its steady-state level is to first polarize protons using the relatively inexpensive TEMPO radical, followed by Hartmann−Hahn cross-polarization to the ^{13}C nuclei. Using this approach, solution polarizations in [1-^{13}C]acetate of >40% (at 1.2 K and 6.7 T) have been achieved in a build-up time of 810 s.[28]

Dissolution. The key innovation introduced by Ardenkjaer-Larsen, Golman, and colleagues and which has made possible medical imaging with ^{13}C-labeled substrates is the dissolution

process, in which the hyperpolarized substrate is brought rapidly to room temperature with minimal loss of polarization.[12] This is achieved by rapidly flushing the sample out of the polarizer magnet using a pressurized superheated solvent (180 °C, ~10 bar). In order to minimize relaxation, it is important to maintain the sample at high magnetic field during the dissolution process and also to avoid zero field during the transfer to the imaging magnet. Because of the dilution that takes place during the dissolution process, it is important that the molecule to be polarized is soluble at high concentration. With the requirement for a long polarization lifetime (long T_1), this puts a further restriction on the molecules that can be polarized and used for imaging *in vivo*.

The majority of ^{13}C-labeled substrates that have been used for metabolic imaging have been hyperpolarized using the dDNP technique.[23,29] An alternative method is parahydrogen-induced polarization (PHIP) (reviewed in ref 30); however, with the exception of succinate,[31] it has not yet been possible to use this technique to hyperpolarize the commonly used ^{13}C-labeled cell substrates. Recently, Aime and co-workers showed that the carboxyl carbons of pyruvate and acetate can be polarized by PHIP by using precursors that contain a hydrogenable functionality.[32] Polarization was then transferred to the carboxyl carbons, and the molecules were cleaved to generate free pyruvate or acetate. In principle, this technique could be extended to other carboxylic acids, further extending the molecules that can be polarized using this method.

Much of the early pre-clinical work used prototype polarizers built in the laboratory of Ardenkjaer-Larsen, Golman, and colleagues or with a commercial derivative manufactured by Oxford Instruments (HyperSense). An adapted version of the prototype polarizer, operated in a clean room adjacent to the MR scanner room, was used in the first clinical trial with hyperpolarized [1-^{13}C]pyruvate in prostate cancer patients.[33] Other polarizers operating on a similar principle have also been described.[34] More recently, researchers at GE have built a polarizer (SPINlab) that, with the appropriate regulatory approval, could be used for clinical studies. The system comprises a closed-cycle, sorption pump-based cryogenic system serviced by a cryo-cooler, which can achieve temperatures of ~1 K and can polarize four samples simultaneously, thus to some extent getting around the problem of long polarization build-up times.[35] Recycling the helium avoids the need for regular refilling as well as reducing costs. The sample to be polarized and the dissolution fluid are placed, under sterile conditions, into a sterile fluid path module that plugs into the polarizer. In the longer term, these "sterile fluid paths" could be made at a remote facility and shipped out to radiology departments, where the polarizer is sited immediately adjacent to the MR scanner. Subsequent polarization, dissolution, and removal of the radical are fully automated, and the polarized sterile sample is then passed through a contactless quality control system, which checks the level of polarization, pH, temperature, and residual radical concentration, before injection into the patient. The original device operated at 3.35 T and produced solid-state polarizations of 35−40%. A later version operates at 5 T.

■ EXTENDING THE POLARIZATION LIFETIME

Short polarization lifetimes have prompted a search for methods that could be used to extend them. One approach is to remove intramolecular dipole−dipole interactions between the ^{13}C label and adjacent protons by deuteration.[18,36] Another

has been to exploit long-lived states that are accessible in coupled spin systems.

Two spin $S = \frac{1}{2}$ nuclei may couple together to form a composite system with total spin $S = 0$ or 1 (Figure 2). If the
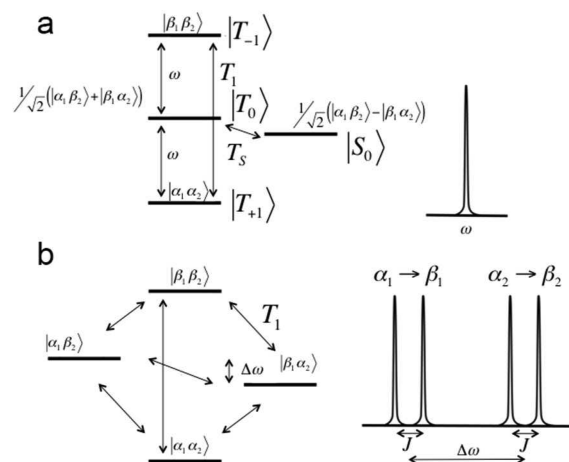

Figure 2. Triplet and singlet states of a magnetically equivalent spin $S = \frac{1}{2}$ pair (a) and the triplet states of a magnetically inequivalent $S = \frac{1}{2}$ pair (b). α and β denote the spin "up" and spin "down" states, respectively. The inequivalent spins, which are weakly coupled, show a difference in chemical shift, $\Delta\omega$, and a spin−spin coupling constant, J. T_1 relaxation processes connect the triplet states, and T_S defines the lifetime of singlet order.

nuclei are in magnetically equivalent environments, then the singlet and triplet states are eigenstates (energy levels) of the system. The $S = 0$ state, which has only one component and is anti-symmetric under exchange of spins, is known as a singlet state and does not give rise to an NMR signal, whereas the $S = 1$ state, which is symmetric, consists of three triplet states that are split by their nuclear resonance frequency. Transitions between the triplet states are governed by T_1 relaxation processes, whereas transitions between the singlet and triplet states occur with a time constant denoted T_S.[37] The dominant T_1 relaxation process for coupled $S = \frac{1}{2}$ nuclei in the solution state is due to dipole−dipole interactions. However, this relaxation mechanism is symmetric with respect to spin exchange and therefore cannot induce singlet−triplet transitions. For this reason, T_S can be very much longer than T_1, and therefore, by depositing polarization in the singlet state, its lifetime can be extended. For a magnetically inequivalent spin pair, where there is a chemical shift difference between them, the singlet−triplet transitions are quenched. Manipulating the magnetic equivalence of a weakly coupled spin pair allows the hyperpolarized signal to be stored in the singlet state of the equivalent system, where exchange symmetry is broken, and then later returned to the NMR-detectable Zeeman states of the inequivalent system, where exchange symmetry is imposed. Starting with an inequivalent two-spin system, a precursor state is prepared that can be used to populate the singlet state as soon as the two spins are made equivalent during a subsequent storage period. This precursor state can be prepared in several different ways (reviewed in ref 37). These include application of resonant radio frequency pulses in a high magnetic field to excite the precursor state, which is then transformed into singlet order following transfer to low field; preparation of singlet order in a high magnetic field using a radio frequency pulse sequence; application of an audio frequency pulse

sequence in a low magnetic field on a pre-polarized sample; and exploitation of chemical reactions that change symmetry. Long-lived states have been created in various hyperpolarized molecules; however, to date, this appears to have been achieved in only two molecules that have been used for metabolic imaging *in vivo*—pyruvate and fumarate.

A study with [2,3-^{13}C]pyruvate showed that singlet order can be generated directly in the dDNP process, without resort to the pulse sequences mentioned above.[38] During dissolution, the high-field eigenstates are adiabatically transformed into the nuclear singlet ($|S_0\rangle$) and triplet ($|T_M\rangle$) eigenstates in the low magnetic field outside the polarizer. For a weakly coupled spin pair with positive gyromagnetic ratio, chemical shift difference, and spin−spin coupling, the correspondence between the low- and high-field states is (see Figure 2) as follows:

$$|\alpha_1\beta_2\rangle \rightarrow |S_0\rangle \qquad |\beta_1\alpha_2\rangle \rightarrow |T_0\rangle \qquad (1)$$

$$|\alpha_2\alpha_2\rangle \rightarrow |T_{+1}\rangle \qquad |\beta_1\beta_2\rangle \rightarrow |T_{-1}\rangle \qquad (2)$$

Nuclear singlet polarization (p_S) corresponds to a mean population difference between the singlet and triplet states, which, neglecting relaxation during transport to low field, is given by

$$p_S = n_{\alpha_1\beta_2} - (n_{\alpha_1\alpha_2} + n_{\beta_1\alpha_2} + n_{\beta_1\beta_2})/3 = -p^2/3 \qquad (3)$$

where n is the population of the indicated spin state. The negative sign arises due to an excess population in the triplet state, depleting the singlet state. Therefore, for 30% polarization, there would be 3% negative singlet polarization. Transfer of the sample back to high field, reversing the transitions shown in eqs 1 and 2, results in observable magnetization. This method for generating the singlet state was used to investigate singlet lifetimes for [2,3-^{13}C]pyruvate in red blood cell suspensions and *in vivo*.[39] Although T_S was longer than T_1 at low fields (several millitesla), it was shorter than T_1 at high fields; moreover, the T_S at low field was not significantly longer than the T_1 at low field of [1-^{13}C]pyruvate. Therefore, in the case of pyruvate, there are relaxation mechanisms that have a strong effect on singlet relaxation, and there is no benefit in generating the singlet state. Nevertheless, observation of singlet polarization in pyruvate was demonstrated *in vivo* following injection of hyperpolarized [2,3-^{13}C]pyruvate into mice.[39]

Clearly, this method of generating singlet polarization is very dependent on the level of polarization that can be achieved. For a polarization of 90%, which can readily be obtained for ^{1}H at 6.7 T and 1.2 K,[28] and which can be transferred to ^{13}C through cross-polarization, the ^{1}H singlet polarization would be 27%. Creating long-lived polarization in ^{1}H, as opposed to ^{13}C, has several benefits. The ^{1}H gyromagnetic ratio is 4-fold greater, and therefore the sensitivity of detection is higher and the imaging gradient strengths required to achieve the same spatial resolution are 4-fold lower. In a clinical context, detection of ^{1}H means that it is not necessary to equip the scanner with ^{13}C spectroscopic capability. Bornet et al.[40] polarized the protons in fumarate and generated singlet order directly. In the polarizer, where the sample is frozen, the protons are magnetically inequivalent; however, following dissolution, when they become magnetically equivalent and exchange symmetry is broken, the singlet state becomes populated. Fumarate, with polarization stored in the singlet state, was added to fumarase, which catalyzes the hydration of fumarate to produce malate. At high magnetic field, the two protons in malate become

magnetically inequivalent, and the singlet polarization in malate is released into observable magnetization. The T_S for the fumarate protons at high field was ∼60 s, which is sufficiently long to make this experiment feasible *in vivo*. However, the experiment was conducted in a Tris-buffered saline solution in D$_2$O, where a deuteron was incorporated into the resulting malate. The T_S in H$_2$O-containing solutions and in more physiologically relevant media, for example in blood, may be much shorter. The benefit of creating this long-lived state in fumarate is that the polarization would be largely preserved following dissolution, injection, and transport in the blood-stream to the tissue of interest, where the polarization in the singlet state would then be released into observable magnet-ization following enzymatic conversion of fumarate into malate.

Although the creation of long-lived states has yet to be used to extend the polarization lifetime *in vivo* of a molecule that would be useful for imaging metabolism, it is nevertheless potentially a very important methodology that may go some way to addressing the fundamental limitation of the dDNP technique. A better understanding of the relaxation mechanisms responsible for singlet-to-triplet conversion may help in identifying molecules that would benefit from this approach.[37]

■ SUBSTRATES USED FOR METABOLIC IMAGING

Pyruvate. [1-^{13}C]Pyruvate has been the most widely used substrate to date and has been the first to transition to the clinic.[33] Following delivery via the circulation, the molecule is rapidly transported into cells on the monocarboxylate trans-porters (MCTs), where flux of ^{13}C label into the endogenous lactate and alanine pools is catalyzed by lactate dehydrogenase (LDH) and alanine aminotransferase, respectively. Sequential spectra acquired from a tumor, following intravenous injection of hyperpolarized [1-^{13}C]pyruvate, show a decaying signal due to loss of the hyperpolarization through spin−lattice relaxation (the T_1 for the carboxyl carbon of pyruvate *in vivo* is ∼30 s) and initially an increasing signal from lactate, due to incorporation of ^{13}C label, followed by T_1 relaxation-dependent decay (see Figure 3). Flux of hyperpolarized ^{13}C label from injected pyruvate into the endogenous lactate pool has been used to grade prostate tumors, with more aggressive tumors showing more lactate labeling,[41] and to detect early responses to drug treatment,[42] where in general lactate labeling is decreased in responding tumors.[23] In the first clinical trial in prostate cancer, lactate labeling was observed in a region of the gland that showed no detectable tumor in T_2- or diffusion-weighted ^{1}H MRI, but which subsequent histological analysis showed contained disease.[33]

Lactate labeling could result both from exchange of the hyperpolarized ^{13}C label between the injected hyperpolarized [1-^{13}C]pyruvate and the endogenous lactate pool and from net conversion of pyruvate into lactate. There is considerable evidence for a significant exchange contribution.[19] In early studies on cells, addition of exogenous lactate increased the rate of lactate labeling.[42] This is incompatible with net flux, since the added lactate will inhibit forward flux through product inhibition of the enzyme,[43] but is consistent with exchange, since it increases the near-equilibrium NADH concentration, which is limiting for the exchange reaction. This is illustrated in Figure 4, which shows the theoretical isotope exchange flux under equilibrium conditions and under conditions where the NADH concentration is fixed. Fitting the calculated isotope exchange fluxes under the former conditions to the Michaelis−Menten equation gives an apparent K_m of LDH for pyruvate of
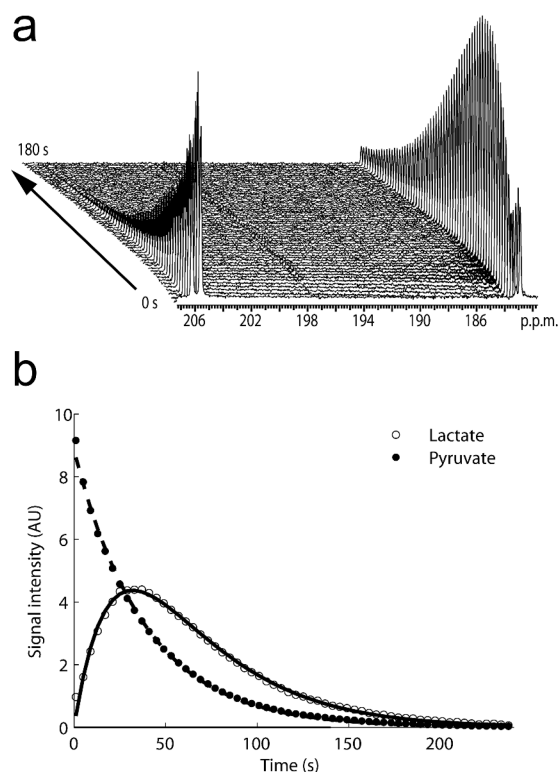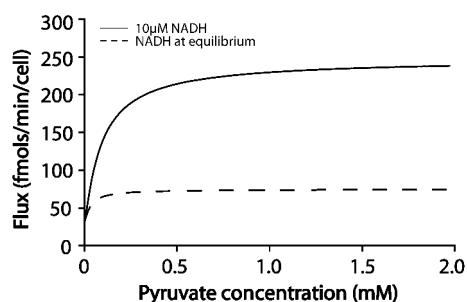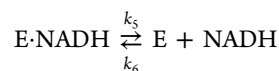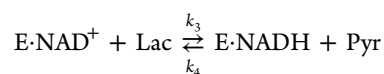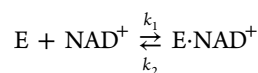
Figure 4. Effect of pyruvate concentration on the calculated LDH isotope exchange velocity (V_{LDH}). The lower curve (dotted line) was calculated assuming an equilibrium NADH concentration. The upper curve (solid line) was calculated by fixing the NADH concentration in the kinetic model at 10 μM. The lactate concentration in the model was 10 mM and the NAD concentration 0.4 mM. The curves were calculated using the following equation:

$$V_{LDH} = \frac{E_0 \left[\frac{k_4 k_6 [H][P]}{k_5} \right]}{\left[1 + \frac{k_6[H]}{k_5} + \frac{k_4 k_6 [H][P]}{k_3 k_5 [L]} \right]}$$

where H represents NADH, P represents pyruvate, and L represents lactate. The equation was derived assuming an ordered ternary complex mechanism for the enzyme (see text). The rate constants were taken from the literature. Reprinted with permission from ref 43. Copyright 2011 American Society for Biochemistry and Molecular Biology.

Figure 3. Exchange of hyperpolarized ^{13}C label between hyperpolarized [1-^{13}C]pyruvate and the endogenous lactate pool in a tumor cell suspension. (a) The [1-^{13}C]lactate signal at 183 ppm shows an initial increase, due to flux of hyperpolarized ^{13}C label from [1-^{13}C]pyruvate, followed by subsequent decay due to T_1-dependent relaxation of the polarization. The signal at 206 ppm is from natural abundance [2-^{13}C]pyruvate, which is a doublet due to coupling with ^{13}C at the C1 position and which decreases due to the loss of polarization. (b) The pyruvate and lactate peak intensities were fit to the modified Bloch equations for two-site exchange in order to determine a first-order rate constant describing flux of ^{13}C label from pyruvate to lactate (k_P) (in the interest of clarity, the pyruvate peak intensity has been reduced by a factor of 100). The modified Bloch equations for two-site exchange are

$$L \underset{k_P}{\overset{k_L}{\rightleftarrows}} P$$

$$dL_z/dt = -\rho_L(L_z - L_\infty) + k_P P_z - k_L L_z$$

$$dP_z/dt = -\rho_P(P_z - P_\infty) + k_L L_z - k_P P_z$$

where L_z and P_z are the z magnetizations of the ^{13}C nucleus in the lactate and pyruvate carboxyl carbons, ρ_L and ρ_P are the spin−lattice relaxation rates ($1/T_{1\,L,P}$), and L_∞ and P_∞ are the equilibrium magnetizations (i.e., at $t = \infty$), which are effectively equivalent to their concentrations. Adapted from ref 42 with permission.

13 μM, whereas the true $K_m = 125$ μM. This low apparent K_m is due to a decrease in the equilibrium NADH concentration as the concentration of pyruvate is increased. If the NADH concentration in the model is fixed at 10 μM, then the isotope exchange rate increases to much higher levels, reflecting the fact that it is limiting for the exchange reaction, and the apparent K_m for pyruvate is increased to 76 μM.

Subsequent studies showed that addition of exogenous lactate also accelerated the observed isotope exchange flux *in vivo*.[44] Exchange was demonstrated directly in tumor cell suspensions by adding [3-^{13}C]pyruvate and detecting the ^{13}C

label in the proton spectrum through splitting of the methyl proton resonances of lactate and pyruvate due to ^{13}C−^{1}H J-coupling. There was no change in the total pyruvate concentration, but there was a decrease in the concentration of [3-^{13}C]pyruvate and an increase in the concentration of [3-^{12}C]pyruvate, again demonstrating exchange of ^{13}C label between pyruvate and lactate.[42] More recently, in experiments with hyperpolarized [1-^{13}C]pyruvate in glioblastoma cells, mass spectrometric measurements on cells to which an equivalent concentration of non-polarized [3-^{13}C]pyruvate had been added showed that there was no increase in the total lactate pool size over the time course of the hyperpolarized experiment, again demonstrating that the observed lactate ^{13}C-labeling was due to exchange rather than net flux.[45] Exchange was demonstrated directly in tumors *in vivo* using a magnetization transfer experiment.[46] Saturation of the hyperpolarized [1-^{13}C]pyruvate resonance resulted in an accelerated decay of the hyperpolarized [1-^{13}C]lactate resonance, demonstrating that there must have been flux of hyperpolarized ^{13}C magnetization from lactate to pyruvate. That the observed label flux is due predominantly to an LDH-catalyzed exchange reaction has important implications for the interpretation of this experiment. LDH has an ordered ternary complex mechanism, where the coenzymes NAD$^+$ and NADH bind first and then lactate and pyruvate, respectively.

$$E + NAD^+ \underset{k_2}{\overset{k_1}{\rightleftarrows}} E\cdot NAD^+$$

$$E\cdot NAD^+ + Lac \underset{k_4}{\overset{k_3}{\rightleftarrows}} E\cdot NADH + Pyr$$

$$E\cdot NADH \underset{k_6}{\overset{k_5}{\rightleftarrows}} E + NADH$$

Exchange of isotope label between lactate and pyruvate can be much faster than between NAD^+ and NADH, and faster therefore than the next chemical flux catalyzed by enzyme, i.e., the metabolically relevant net conversion of pyruvate and NADH to lactate and NAD^+.[19]

Several kinetic models have been used to analyze exchange of hyperpolarized ^{13}C label between injected [1-^{13}C]pyruvate and the endogenous lactate pool. The first used fitting of the pyruvate and lactate signal intensities to the modified Bloch equations for two-site exchange and ignored the effects of pyruvate delivery (Figure 3).[42] A recent comparison with more complex models concluded that this simple two-site exchange model, and even simpler unidirectional models, are sufficient to estimate the first-order rate constant, k_P, describing label flux between pyruvate and lactate.[45] Another approach, which does not require curve fitting, is to take the ratio of the areas under the lactate and pyruvate signal intensity curves, which was shown to be proportional to k_P.[47] An added advantage of this analysis was that it was found to be independent of the pyruvate arterial input function (AIF), although direct measurements of the pyruvate AIF have shown that it has little influence on estimates of k_P.[48] However, while estimates of k_P appear to be robust, the key problem is that, without an estimate of pyruvate concentration in the tissue, we are unable to determine a metabolically relevant value for the isotope flux. While measuring a first-order rate constant and changes in this rate constant with various interventions may be adequate in pre-clinical animal studies, where the tissues are effectively identical and the pyruvate concentration delivered to the tissue may be very reproducible, this may be more of a problem in the clinic. Although absolute measurements of flux in the clinic may be difficult, it may be sufficient simply to measure changes in the rate constant before and after an intervention, for example tumor treatment.

Analyzing exchange data using the modified Bloch equations for two-site exchange, or variants of these equations, assumes that there is no loss of polarization in enzyme−substrate complexes, for example in the LDH·NAD^+·lactate and LDH·NADH·pyruvate ternary complexes. The concentrations of these enzyme−substrate complexes are small when compared with the free substrate concentrations, and consequently they are turning over so rapidly that their lifetimes are short when compared with the polarization lifetime. Therefore, there is little opportunity for loss of polarization.[49] This will be the case even if the polarization lifetime is shortened in an on-enzyme complex.

Studies on the dependence of the exchange rate on pyruvate concentration in isolated cells[43,50] and in vivo[51] implied that the exchange velocity must depend on MCT as well as LDH activity. The observed apparent K_m was similar to that for pyruvate transport and much higher than the K_m of LDH for pyruvate in the exchange reaction (see Figure 4).[43] More recent studies have demonstrated the importance of MCT activity for the exchange. In breast cancer (MCF7) cells treated with a mitogen-activated protein kinase inhibitor, there was a 31% decrease in label flux, whereas in prostate cancer (PC3) cells, there was a 167% increase. LDH expression and lactate concentration were increased in both cell lines following drug treatment. The decrease in exchange in the MCF7 cells was explained by a decrease in MCT1 expression that was not observed in the PC3 cells.[52] In a bioreactor study with perifused metastatic and non-metastatic renal carcinoma cells, the metastatic cells showed an apparently lower rate of lactate

labeling. This was explained by higher expression of MCT1 in the metastatic cells, which led to more rapid export of labeled lactate and loss from the sensitive region of the NMR coil.[53] Application of metabolic control analysis showed that, in murine lymphoma cells, control of isotope flux was shared nearly equally between the membrane transporters and LDH.[43] A similar analysis could potentially be performed in vivo by using PI3K inhibitors to selectively lower the expression of LDH and then determining the effects on the exchange rate.[43,54] Another approach would be to use diffusion weighting to localize the pyruvate and lactate signals to the intra- and extracellular spaces and thus to examine the effects of transport more directly. In the murine lymphoma model, diffusion measurements in vivo showed that most of the labeled lactate formed from hyperpolarized [1-^{13}C]pyruvate was intracellular over the time course of the experiment.[55] In a diffusion-weighted spin echo experiment with hyperpolarized [1-^{13}C]-lactate, there was a progressive increase in signal intensity, which measurements in the presence of an MCT inhibitor showed was due in small part to tumor cell uptake and in larger part to extravasation of the labeled lactate.

Measurements of hyperpolarized ^{13}C label exchange between injected pyruvate and endogenous lactate are ideally suited to tumor imaging since the lactate pool size is often large, due to the high levels of aerobic glycolysis displayed by tumors (the "Warburg effect")[56,57] and the high levels of expression of the MCTs and LDH. The highly interconnected nature of metabolic pathways, which form "scale-free" networks, means that this isotope flux is likely to be affected by disparate interventions that affect any part of the metabolic network[58] and probably explains why nearly all studies have reported some effect of tumor treatment on this flux.[23] A corollary is that, in order to understand what the observed changes in flux mean, it is important to have a thorough understanding of the underlying mechanism. For example, whereas an MCT inhibitor might be expected to decrease the exchange through inhibition of pyruvate uptake, this might be offset if the inhibitor also leads to an increase in the steady-state endogenous lactate concentration. Which effect predominates will depend on the relative flux control coefficients of the MCTs and LDH for the exchange, which are likely to vary between different tumor types.

Treatment response is usually detected in the clinic by looking for evidence of reductions in tumor size using anatomical imaging with CT or MRI. However, these morphological changes may take weeks or even months to become apparent and may not happen at all with cytostatic therapies.[59] Imaging changes in metabolism can give a much earlier indication of whether a drug is engaging with its target, enabling ineffective treatments to be abandoned and providing an opportunity to try alternatives earlier during the course of the disease.[59] Positron emission tomography (PET) measurements with the glucose analogue, ^{18}F-labeled fluorodeoxyglucose (FDG), and its increased uptake by tumors are already widely used in the clinic to detect and grade tumors and to monitor their response to treatment.[59] Since the FDG-PET and hyperpolarized [1-^{13}C]pyruvate experiment have been shown to be similarly sensitive for detecting early evidence of treatment response in a murine lymphoma model,[60] it is pertinent to ask what advantages the hyperpolarized [1-^{13}C]-pyruvate experiment might have over the FDG-PET experiment in the clinic. The hyperpolarized [1-^{13}C]pyruvate experiment could be used multiple times in an iterative

approach to select the best drug or drug combination to treat an individual patient, whereas with FDG-PET the exposure to ionizing radiation may limit the number of times that a patient could be imaged. Another advantage of imaging with hyperpolarized [1-^{13}C]pyruvate is that it can be used in tumors where PET imaging of FDG uptake is problematic, for example in brain tumors, where high levels of FDG uptake in surrounding brain tissue can make detection of tumor uptake difficult, and in the prostate, where low uptake in prostate tumors can be masked by high signal from the adjacent bladder.[59] The disadvantage of imaging with hyperpolarized [1-^{13}C]pyruvate is that the short lifetime of the polarization prevents extensive imaging beyond the immediate vicinity of the primary tumor, whereas the sensitivity of FDG-PET combined with whole-body imaging makes it a very effective tool for detecting distant metastases.[61] Another disadvantage of the hyperpolarized pyruvate experiment is that it requires injection of supra-physiological pyruvate concentrations. For example, the normal concentration of pyruvate in human blood is ~50 μM,[62] whereas in the clinical trial in prostate cancer hyperpolarized [1-^{13}C]pyruvate was injected at a plasma concentration of ~1.5 mM.[33] Although there was no evidence of toxicity, it would clearly be desirable to inject the labeled molecule at more physiological concentrations. Since the observed label flux is due predominantly to an exchange reaction and lactate is present in human blood at concentrations of 1−5 mM, this could be achieved by injecting hyperpolarized [1-^{13}C]lactate instead of pyruvate and observing labeling in the endogenous pyruvate pool. However, this experiment gives much less signal because the pyruvate pool is very small when compared to the lactate pool.[62] An alternative is to observe exchange of deuterium label between injected hyperpolarized [2-^{2}H,1-^{13}C]lactate and the endogenous lactate pool, where the deuterium label is detected via the spin-coupled hyperpolarized ^{13}C label in a heteronuclear spin echo experiment (see Figure 5).[62] The phase of the echo indicates whether the observed hyperpolarized [1-^{13}C]lactate is protonated at the C-2 position, and the amplitude of the echo, when compared to the signal obtained after the first low flip angle pulse in the sequence, can potentially indicate the location of the labeled lactate, particularly if the sequence is diffusion-weighted. When this experiment was performed in a murine lymphoma model, there was a progressive increase in the echo amplitude, mainly due to extravasation of the labeled lactate and in part due to tumor cell uptake. As well as dispensing with the need for an unphysiologically high pyruvate concentration, this experiment, which interrogates the same biochemistry as the pyruvate experiment, also simplifies imaging since there is no change in chemical shift. The lactate labeling is determined simply from the phase of the single observed ^{13}C resonance.

Although imaging is likely to continue to play an important role in monitoring the responses of tumors to treatment in the clinic, it now seems likely that it will be used alongside other non-invasive methods for assessment of treatment response. An important new development in this regard has been the analysis of circulating tumor DNA (ctDNA) in the plasma, which was shown to be capable of detecting response in breast tumors before there were any changes in tumor size, determined by conventional morphological imaging.[63] Sequencing of ctDNA has also been used to monitor the evolution of treatment resistance.[64] This is a powerful new technology that needs to be evaluated in comparison with functional imaging methods, such
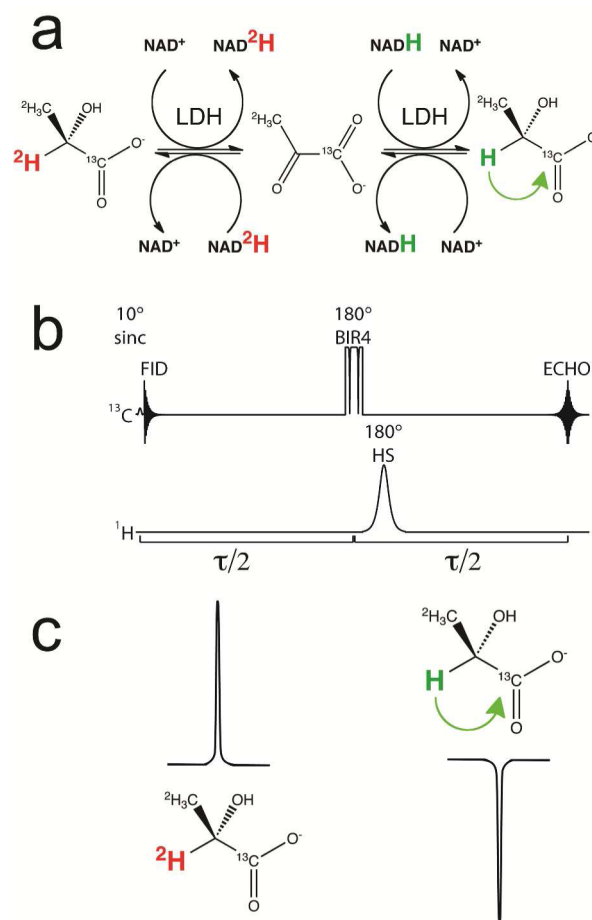

Figure 5. Assessing lactate dehydrogenase activity by measuring hydrogen/deuterium exchange in hyperpolarized L-[1-^{13}C,U-^{2}H]-lactate. a) Scheme showing exchange of the C-2 deuterium label in hyperpolarized L-[1-^{13}C,U-^{2}H]lactate for protons from the endogenous NADH pool and, ultimately, from the endogenous lactate pool. Application of a ^{1}H 180° pulse in a heteronuclear spin echo experiment (with $\tau = 1/J \approx 310$ ms) results in phase inversion of the hyperpolarized ^{13}C signal from lactate that has a proton at the C-2 position. Adapted from ref 62 with permission.

as the metabolic imaging methods described here, which can give a much earlier indication of treatment response.

In tissues with high mitochondrial activity, such as heart muscle, [1-^{13}C]pyruvate is decarboxylated in the reaction catalyzed by pyruvate dehydrogenase (PDH) to produce ^{13}CO$_2$. The labeled CO$_2$ is in exchange with bicarbonate, and at physiological pHs most of this labeled CO$_2$ will be observed as H^{13}CO$_3^-$. In systems where there is sufficient carbonic anhydrase activity and the ^{13}CO$_2$ and H^{13}CO$_3^-$ pools reach isotopic equilibrium, the ^{13}CO$_2$/H^{13}CO$_3^-$ signal ratio can be used to estimate pH.[65,66] In perfused hearts, PDH flux was shown to be modulated by the availability of fatty acids[67] and in vivo by fasting and diabetes.[68] Temporary coronary occlusion in the pig heart in vivo led to a loss of H^{13}CO$_3^-$ production, indicating a decrease in PDH activity, despite restoration of perfusion, as indicated by contrast agent enhanced MRI and by the delivery of pyruvate and subsequent labeling of alanine and lactate.[69] Further studies suggest that these experiments with [1-^{13}C]pyruvate in the heart should translate to the clinic.[70] Hyperpolarized [2-^{13}C]pyruvate resulted in labeling of [1-^{13}C]-acetylcarnitine, [5-^{13}C]citrate, and [5-^{13}C]glutamate in the

perfused heart, which was decreased following ischemia and reperfusion.[71] However, this labeled form of pyruvate is unlikely to translate to the clinic due to the low signal intensities of its labeled metabolites. The primary fate of hyperpolarized $[1\text{-}^{13}C]$pyruvate in the perfused liver was shown to be carboxylation, rather than oxidation by PDH, which resulted in labeling of malate and aspartate. The $H^{13}CO_3^-$ that was observed was produced via the gluconeogenic enzyme, phosphoenolpyruvate carboxykinase.[72] However, in the liver, *in vivo* production of $H^{13}CO_3^-$ seems to be predominantly via PDH.[23]

Fumarate. The primary aim of cancer treatment is to selectively kill tumor cells. Hyperpolarized $[1\text{-}^{13}C]$pyruvate has the potential to show whether a drug has hit its target in a tumor; hyperpolarized $[1,4\text{-}^{13}C]$fumarate can show whether there is subsequent cell death. Fumarate uptake by cells is slow on the time scale of the polarization. However, when a cell dies and becomes necrotic and the plasma membrane becomes leaky, fumarate can enter the cell rapidly, or the enzyme fumarase can leak out, and fumarase can then catalyze the rapid hydration of fumarate to produce malate. Detection of malate, following injection of hyperpolarized $[1,4\text{-}^{13}C]$fumarate, appears to be a sensitive indicator of necrotic cell death,[73] detecting relatively low levels of diffuse cell death.[74] This substrate is also likely to translate to the clinic, where it could be used to detect cell death in tumors post treatment, and potentially also in other tissues where disease is present.[75]

Glucose. PET measurements of FDG uptake interrogate just three steps in carbohydrate metabolism: delivery via the bloodstream, cell uptake on the glucose transporters, and subsequent phosphorylation and trapping in the reaction catalyzed by hexokinase. Both the glucose transporters and hexokinase activity are frequently up-regulated in tumors. Measurements with polarized $[1\text{-}^{13}C]$pyruvate also interrogates just three steps: delivery via the circulation, cell uptake on the MCTs, and subsequent isotope exchange in the reaction catalyzed by LDH. In tumors, expression of LDH and the MCTs is also often increased. Combining these two experiments using a PET/MR machine has the potential to examine flux in the entire glycolytic pathway. This can also be achieved by using hyperpolarized $[U\text{-}^{13}C,U\text{-}^2H]$glucose. Deuteration increases the T_1's of the glucose carbons from <1 to ~10 s and has allowed measurements of label flux from glucose to lactate. Measurements with hyperpolarized $[U\text{-}^{13}C,U\text{-}^2H]$-glucose have been made in *E. coli*,[14] yeast,[15] and tumor cells *in vitro*,[16,17] and have also been performed in a tumor model *in vivo*,[18] where flux was decreased following drug treatment. As well as signal from lactate, signals from glycolytic intermediates and a pentose phosphate pathway intermediate, 6-phospho-gluconate, were also observed[24] (Figure 1). The latter offers the possibility of real-time flux measurements in a pathway that is responsible, through the generation of NADPH, for resistance to oxidative stress and which is associated with tumor aggressiveness and resistance to treatment. Although hyper-polarized $[U\text{-}^{13}C,U\text{-}^2H]$glucose can provide unique information about real-time pathway fluxes, the short half-life of the polarization will make it challenging to translate to the clinic, unless ways can be found to deliver the labeled glucose more rapidly to the tissue of interest.

Ascorbate and Dehydroascorbate. Ascorbate (AA) buffers reactive oxygen species (ROS), such as superoxide and hydrogen peroxide, by reducing them and, in the process, is oxidized to dehydroascorbic acid (DHA). Extracellular DHA is transported into cells on the glucose transporters where it is reduced to AA. The C-1-labeled molecules have long T_1's and polarize well.[76,77] Despite tumors having a high ROS load, injection of hyperpolarized $[1\text{-}^{13}C]$AA into tumor-bearing mice resulted in no detectable oxidation in the tumor.[76] However, injection of $[1\text{-}^{13}C]$DHA into tumor-bearing animals resulted in rapid reduction of DHA to AA in the tumors,[76,77] and also in other tissues, including kidneys, liver, and brain.[78] This may partly explain why very little tumor oxidation of AA was observed. The rate of DHA reduction may report on the capacity of the tumor cell to resist oxidative stress. However, DHA results in transient respiratory suppression, and therefore it is unlikely that this substrate will translate to the clinic.

IMAGING

The polarization is non-recoverable, and therefore efficient use must be made of it in generating an image. Moreover, for molecules like pyruvate, where the useful information is in the kinetics of exchange, and for molecules like fumarate, where we cannot know *a priori* when the maximum malate signal will be observed, it is desirable to collect a series of rapidly acquired images. Various pulse sequences have been developed that satisfy these requirements and are expected to produce image resolutions in the clinic of ~5 mm (reviewed in ref 21). Spiral chemical shift imaging, in which spiral readout gradients sample the x and y dimensions simultaneously and in which the spiral gradients are concatenated multiple times for chemical shift encoding, can be used to generate 2D spectroscopic images of a single slice in less than 1 s.[13] An iterative least-squares chemical shift based method, which requires prior information about the chemical shifts of the labeled compounds and that takes advantage of the sparsity of the hyperpolarized ^{13}C spectrum, can be used to minimize the number of excitations required for spectral decomposition.[79] Echo planar spectroscopic imaging sequences and compressed sensing have also been used to accelerate image acquisition.[80] An alternative to spectroscopically resolving the labeled metabolites is to excite each one individually using spectral−spatial pulses.[81] Multi-band spectral−spatial pulses can be used to minimally excite the injected labeled substrate with a low flip angle, preserving the reservoir of polarization in the tissue, while exciting the less intense resonances from the labeled metabolites produced from it with larger flip angle pulses.[80]

Tumor heterogeneity has been correlated with therapeutic resistance and subsequent relapse,[82] and clearly imaging heterogeneity with hyperpolarized ^{13}C-labeled substrates would be of considerable interest. For example, different clones in a tumor that express different oncogenes may present distinct metabolic signatures that could be imaged. However, in some cases imaging within the tumor may be unnecessary, and it may be sufficient to know only that the signal arises from the tumor itself. For example, since fumarate is a positive contrast agent, which detects dead cells through the production of malate, imaging at low resolution will enhance the detection of low levels of diffuse cell death.

CONCLUDING REMARKS

While hyperpolarized ^{13}C-labeled cell substrates can be used to make unique measurements in pre-clinical studies, arguably the true power of this technique lies in its capability to make these measurements in the clinic. The completion of the first clinical trial in prostate cancer has demonstrated that the technique will

produce detectable signals in tumors; the key question now is whether it will find an important clinical application, which affects clinical decision-making and changes the way we treat patients. One can speculate in general terms what these applications might be. Pathologies are often characterized by ischemia, hypoxia, and inflammation, with attendant increases in tissue lactate concentration and LDH activities. Therefore, in principle, the presence of many diseases, and their responses to treatment, could be detected using hyperpolarized [1-^{13}C]-pyruvate. The presence of disease is also often associated with cell death; for example, tumors frequently host high levels of dead cells. Therefore, disease and response to treatment should also be detectable with hyperpolarized [1,4-^{13}C]fumarate. FDG has been a commercial and clinical success, because it gives good contrast and, unlike many PET tracers, it can be used in many different disease settings. Perhaps pyruvate and fumarate will be the equivalent tracers of the dDNP world, applicable for detection and treatment response monitoring in many different diseases.

■ AUTHOR INFORMATION

Corresponding Author
*kmb1001@cam.ac.uk

■ REFERENCES

(1) Johnson, G. A.; Benveniste, H.; Black, R. D.; Hedlund, L. W.; Maronpot, R. R.; Smith, B. R. *Magn. Reson. Q.* **1993**, *9*, 1.
(2) Nelson, S. J. *NMR Biomed.* **2011**, *24*, 734.
(3) Shulman, R. G.; Rothman, D. L. *Annu. Rev. Physiol.* **2001**, *63*, 15.
(4) Brindle, K. M. *Prog. Nucl. Magn. Reson. Spectrosc.* **1988**, *20*, 257.
(5) Shulman, R. G.; Brown, T. R.; Ugurbil, K.; Ogawa, S.; Cohen, S. M.; den Hollander, J. A. *Science* **1979**, *205*, 160.
(6) den Hollander, J. A.; Ugurbil, K.; Brown, T. R.; Shulman, R. G. *Biochemistry* **1981**, *20*, 5871.
(7) Jeffrey, F. M.; Rajagopal, A.; Malloy, C. R.; Sherry, A. D. *Trends Biochem. Sci.* **1991**, *16*, 5.
(8) DeBerardinis, R. J.; Mancuso, A.; Daikhin, E.; Nissim, I.; Yudkoff, M.; Wehrli, S.; Thompson, C. B. *Proc. Natl. Acad. Sci. U.S.A.* **2007**, *104*, 19345.
(9) Mashimo, T.; Pichumani, K.; Vemireddy, V.; Hatanpaa, K. J.; Singh, D. K.; Sirasanagandla, S.; Nannepaga, S.; Piccirillo, S. G.; Kovacs, Z.; Foong, C.; Huang, Z.; Barnett, S.; Mickey, B. E.; DeBerardinis, R. J.; Tu, B. P.; Maher, E. A.; Bachoo, R. M. *Cell* **2014**, *159*, 1603.
(10) Brindle, K. M.; Boyd, J.; Campbell, I. D.; Porteous, R.; Soffe, N. *Biochem. Biophys. Res. Commun.* **1982**, *109*, 864.
(11) Rothman, D. L.; Behar, K. L.; Hetherington, H. P.; den Hollander, J. A.; Bendall, M. R.; Petroff, O. A.; Shulman, R. G. *Proc. Natl. Acad. Sci. U.S.A.* **1985**, *82*, 1633.
(12) Ardenkjaer-Larsen, J. H.; Fridlund, B.; Gram, A.; Hansson, G.; Hansson, L.; Lerche, M. H.; Servin, R.; Thaning, M.; Golman, K. *Proc. Natl. Acad. Sci. U.S.A.* **2003**, *100*, 10158.
(13) Mayer, D.; Yen, Y. F.; Tropp, J.; Pfefferbaum, A.; Hurd, R. E.; Spielman, D. M. *Magn. Reson. Med.* **2009**, *62*, 557.
(14) Meier, S.; Jensen, P. R.; Duus, J. Ø. *FEBS Lett.* **2011**, *585*, 3133.
(15) Meier, S.; Karlsson, M.; Jensen, P. R.; Lerche, M. H.; Duus, J. O. *Mol. Biosystems* **2011**, *7*, 2834.
(16) Harris, T.; Degani, H.; Frydman, L. *NMR Biomed.* **2013**, *26*, 1831.
(17) Christensen, C. E.; Karlsson, M.; Winther, J. R.; Jensen, P. R.; Lerche, M. H. *J. Biol. Chem.* **2014**, *289*, 2344.
(18) Rodrigues, T. B.; Serrao, E. M.; Kennedy, B. W. C.; Hu, D.-E.; Kettunen, M. I.; Brindle, K. M. *Nat. Med.* **2014**, *20*, 93.
(19) Brindle, K. M.; Bohndiek, S. E.; Gallagher, F. A.; Kettunen, M. I. *Magn. Reson. Med.* **2011**, *66*, 505.
(20) Kurhanewicz, J.; Vigneron, D.; Brindle, K.; Chekmenev, E.; Comment, A.; Cunningham, C.; DeBerardinis, R.; Green, G.; Leach, M.; Rajan, S.; Rizi, R.; Ross, B.; Warren, W.; Malloy, C. *Neoplasia* **2011**, *13*, 81.
(21) Hurd, R. E.; Yen, Y. F.; Chen, A.; Ardenkjaer-Larsen, J. H. *J. Magn. Reson. Imaging* **2012**, *36*, 1314.
(22) Keshari, K. R.; Wilson, D. M. *Chem. Soc. Rev.* **2014**, *43*, 1627.
(23) Comment, A.; Merritt, M. E. *Biochemistry* **2014**, *53*, 7333.
(24) Timm, K. N.; Hartl, J.; Keller, M. A.; Hu, D.-E.; Kettunen, M. I.; Rodrigues, T. B.; Ralser, M.; Brindle, K. M. *Magn. Reson. Med.* **2014**, DOI: 10.1002/mrm.25561.
(25) Ardenkjaer-Larsen, J. H.; Macholl, S.; Jóhannesson, H. *Appl. Magn. Reson.* **2008**, *34*, 509.
(26) Eichhorn, T. R.; Takado, Y.; Salameh, N.; Capozzi, A.; Cheng, T.; Hyacinthe, J.-N.; Mishkovsky, M.; Roussel, C.; Comment, A. *Proc. Natl. Acad. Sci. U.S.A.* **2013**, *110*, 18064.
(27) Lumata, L.; Kovacs, Z.; Malloy, C.; Sherry, A. D.; Merritt, M. *Phys. Med. Biol.* **2011**, *56*, N85.
(28) Bornet, A.; Melzi, R.; Perez Linde, A. J.; Hautle, P.; van den Brandt, B.; Jannin, S.; Bodenhausen, G. *J. Phys. Chem. Lett.* **2013**, *4*, 111.
(29) Keshari, K. R.; Wilson, D. M. *Chem. Soc. Rev.* **2014**, *43*, 1627.
(30) Duckett, S. B.; Mewis, R. E. *Acc. Chem. Res.* **2012**, *45*, 1247.
(31) Bhattacharya, P.; Chekmenev, E. Y.; Perman, W. H.; Harris, K. C.; Lin, A. P.; Norton, V. A.; Tan, C. T.; Ross, B. D.; Weitekamp, D. P. *J. Magn. Reson.* **2007**, *186*, 150.
(32) Reineri, F.; Boi, T.; Aime, S. *Nat. Commun.* **2015**, DOI: 10.1038/ncomms6858.
(33) Nelson, S. J.; Kurhanewicz, J.; Vigneron, D. B.; Larson, P. E. Z.; Harzstark, A. L.; Ferrone, M.; van Criekinge, M.; Chang, J. W.; Bok, R.; Park, I.; Reed, G.; Carvajal, L.; Small, E. J.; Munster, P.; Weinberg, V. K.; Ardenkjaer-Larsen, J. H.; Chen, A. P.; Hurd, R. E.; Odegardstuen, L.-I.; Robb, F. J.; Tropp, J.; Murray, J. A. *Sci. Transl. Med.* **2013**, *5*, 198ra108.
(34) Brandt, B. v. d.; Kurdzesau, F.; Jannin, S.; Konter, J. A.; Hautle, P.; Wenckebach, W. T.; Gruetter, R.; Klink, J. J. v. d. *Concepts Magn. Reson. B: Magn. Reson. Eng.* **2007**, *31B*, 255.
(35) Ardenkjaer-Larsen, J. H.; Leach, A. M.; Clarke, N.; Urbahn, J.; Anderson, D.; Skloss, T. W. *NMR Biomed.* **2011**, *24*, 927.
(36) Allouche-Arnon, H.; Lerche, M. H.; Karlsson, M.; Lenkinski, R. E.; Katz-Brull, R. *Contrast Media Mol. Imaging* **2011**, *6*, 499.
(37) Levitt, M. H. *Annu. Rev. Phys. Chem.* **2012**, *63*, 89.
(38) Tayler, M. C. D.; Marco-Rius, I.; Kettunen, M. I.; Brindle, K. M.; Levitt, M. H.; Pileio, G. *J. Am. Chem. Soc.* **2012**, *134*, 7668.
(39) Marco-Rius, I.; Tayler, M. C. D.; Kettunen, M. I.; Larkin, T. J.; Timm, K. N.; Serrao, E. M.; Rodrigues, T. B.; Pileio, G.; Ardenkjaer-Larsen, J. H.; Levitt, M. H.; Brindle, K. M. *NMR Biomed.* **2013**, *26*, 1696.
(40) Bornet, A.; Ji, X.; Mammoli, D.; Vuichoud, B.; Milani, J.; Bodenhausen, G.; Jannin, S. *Chem.—Eur. J.* **2014**, *20*, 17113.
(41) Albers, M. J.; Bok, R.; Chen, A. P.; Cunningham, C. H.; Zierhut, M. L.; Zhang, V. Y.; Kohler, S. J.; Tropp, J.; Hurd, R. E.; Yen, Y. F.; Nelson, S. J.; Vigneron, D. B.; Kurhanewicz, J. *Cancer Res.* **2008**, *68*, 8607.

(42) Day, S. E.; Kettunen, M. I.; Gallagher, F. A.; Hu, D. E.; Lerche, M.; Wolber, J.; Golman, K.; Ardenkjaer-Larsen, J. H.; Brindle, K. M. *Nature Med.* **2007**, *13*, 1382.

(43) Witney, T. H.; Kettunen, M. I.; Brindle, K. M. *J. Biol. Chem.* **2011**, *286*, 24572.

(44) Hurd, R. E.; Spielman, D.; Josan, S.; Yen, Y. F.; Pfefferbaum, A.; Mayer, D. *Magn. Reson. Med.* **2013**, *70*, 936.

(45) Harrison, C.; Yang, C.; Jindal, A.; DeBerardinis, R. J.; Hooshyar, M. A.; Merritt, M.; Sherry, A. D.; Malloy, C. R. *NMR Biomed.* **2012**, *25*, 1286.

(46) Kettunen, M. I.; Hu, D.-E.; Witney, T. H.; McLaughlin, R.; Gallagher, F. A.; Bohndiek, S. E.; Day, S. E.; Brindle, K. M. *Magn. Reson. Med.* **2010**, *63*, 872.

(47) Hill, D. K.; Orton, M. R.; Mariotti, E.; Boult, J. K. R.; Panek, R.; Jafar, M.; Parkes, H. G.; Jamin, Y.; Miniotis, M. F.; Al-Saffar, N. M. S.; Beloueche-Babari, M.; Robinson, S. P.; Leach, M. O.; Chung, Y. L.; Eykyn, T. R. *PLoS One* **2013**, *8*, 9.

(48) Kazan, S. M.; Reynolds, S.; Kennerley, A.; Wholey, E.; Bluff, J. E.; Berwick, J.; Cunningham, V. J.; Paley, M. N.; Tozer, G. M. *Magn. Reson. Med.* **2013**, *70*, 943.

(49) Brindle, K. M.; Radda, G. K. *Biochim. Biophys. Acta* **1985**, *829*, 188.

(50) Harris, T.; Eliyahu, G.; Frydman, L.; Degani, H. *Proc. Natl. Acad. Sci. U.S.A.* **2009**, *106*, 18131.

(51) Zierhut, M. L.; Yen, Y. F.; Chen, A. P.; Bok, R.; Albers, M. J.; Zhang, V.; Tropp, J.; Park, I.; Vigneron, D. B.; Kurhanewicz, J.; Hurd, R. E.; Nelson, S. J. *J. Magn. Reson.* **2009**, *202*, 85.

(52) Lodi, A.; Woods, S. M.; Ronen, S. M. *NMR Biomed.* **2013**, *26*, 299.

(53) Keshari, K. R.; Sriram, R.; Koelsch, B. L.; Van Criekinge, M.; Wilson, D. M.; Kurhanewicz, J.; Wang, Z. J. *Cancer Res.* **2013**, *73*, 529.

(54) Ward, C. S.; Venkatesh, H. S.; Chaumeil, M. M.; Brandes, A. H.; VanCriekinge, M.; Dafni, H.; Sukumar, S.; Nelson, S. J.; Vigneron, D. B.; Kurhanewicz, J.; James, C. D.; Haas-Kogan, D. A.; Ronen, S. M. *Cancer Res.* **2010**, *70*, 1296.

(55) Kettunen, M.; Kennedy, B.; Hu, D.-E.; Brindle, K. *Magn. Reson. Med.* **2012**, *70*, 1200.

(56) Gatenby, R. A.; Gillies, R. J. *Nature Rev. Cancer* **2004**, *4*, 891.

(57) vander Heiden, M. G.; Cantley, L. C.; Thompson, C. B. *Science* **2009**, *324*, 1029.

(58) Brindle, K. In *Metabolic Engineering in the Post Genomic Era*; Kholodenko, B., Westerhoff, H. V., Eds.; Horizon Bioscience, UK, 2004.

(59) Brindle, K. *Nat. Rev. Cancer* **2008**, *8*, 94.

(60) Witney, T.; Kettunen, M.; Day, S.; Hu, D.; Neves, A.; Gallagher, F.; Fulton, S.; Brindle, K. *Neoplasia* **2009**, *6*, 574.

(61) Juweid, M.; Cheson, B. *N. Engl. J. Med.* **2006**, *354*, 496.

(62) Kennedy, B. W. C.; Kettunen, M. I.; Hu, D.-E.; Brindle, K. M. *J. Am. Chem. Soc.* **2012**, *134*, 4969.

(63) Dawson, S. J.; Tsui, D. W. Y.; Murtaza, M.; Biggs, H.; Rueda, O. M.; Chin, S. F.; Dunning, M. J.; Gale, D.; Forshew, T.; Mahler-Araujo, B.; Rajan, S.; Humphray, S.; Becq, J.; Halsall, D.; Wallis, M.; Bentley, D.; Caldas, C.; Rosenfeld, N. *N. Engl. J. Med.* **2013**, *368*, 1199.

(64) Murtaza, M.; Dawson, S. J.; Tsui, D. W. Y.; Gale, D.; Forshew, T.; Piskorz, A. M.; Parkinson, C.; Chin, S. F.; Kingsbury, Z.; Wong, A. S. C.; Marass, F.; Humphray, S.; Hadfield, J.; Bentley, D.; Chin, T. M.; Brenton, J. D.; Caldas, C.; Rosenfeld, N. *Nature* **2013**, *497*, 108.

(65) Gallagher, F.; Kettunen, M.; Day, S.; Hu, D.-E.; Ardenkjær-Larsen, J.; in 't Zandt, R.; Jensen, P.; Karlsson, M.; Golman, K.; Lerche, M.; Brindle, K. *Nature* **2008**, *453*, 940.

(66) Gallagher, F. A.; Kettunen, M. I.; Brindle, K. M. *NMR Biomed.* **2011**, *24*, 1006.

(67) Merritt, M. E.; Harrison, C.; Storey, C.; Jeffrey, F. M.; Sherry, A. D.; Malloy, C. R. *Proc. Natl. Acad. Sci. U.S.A.* **2007**, *104*, 19773.

(68) Schroeder, M. A.; Cochlin, L. E.; Heather, L. C.; Clarke, K.; Radda, G. K.; Tyler, D. J. *Proc. Natl. Acad. Sci. U.S.A.* **2008**, *105*, 12051.

(69) Golman, K.; Petersson, J. S.; Magnusson, P.; Johansson, E.; Åkeson, P.; Chai, C.-M.; Hansson, G.; Månsson, S. *Magn. Reson. Med.* **2008**, *59*, 1005.

(70) Lau, A. Z.; Chen, A. P.; Ghugre, N. R.; Ramanan, V.; Lam, W. W.; Connelly, K. A.; Wright, G. A.; Cunningham, C. H. *Magn. Reson. Med.* **2010**, *64*, 1323.

(71) Schroeder, M. A.; Atherton, H. J.; Ball, D. R.; Cole, M. A.; Heather, L. C.; Griffin, J. L.; Clarke, K.; Radda, G. K.; Tyler, D. J. *FASEB J.* **2009**, *23*, 2529.

(72) Merritt, M. E.; Harrison, C.; Sherry, A. D.; Malloy, C. R.; Burgess, S. C. *Proc. Natl. Acad. Sci. U.S.A.* **2011**, *108*, 19084.

(73) Gallagher, F. A.; Kettunen, M. I.; Hu, D. E.; Jensen, P. R.; Zandt, R. I.; Karlsson, M.; Gisselsson, A.; Nelson, S. K.; Witney, T. H.; Bohndiek, S. E.; Hansson, G.; Peitersen, T.; Lerche, M. H.; Brindle, K. M. *Proc. Natl. Acad. Sci. U.S.A.* **2009**, *106*, 19801.

(74) Bohndiek, S. E.; Kettunen, M. I.; Hu, D. E.; Witney, T. H.; Kennedy, B. W. C.; Gallagher, F. A.; Brindle, K. M. *Mol. Cancer Therapeutics* **2010**, *9*, 3278.

(75) Clatworthy, M. R.; Kettunen, M. I.; Hu, D. E.; Mathews, R. J.; Witney, T. H.; Kennedy, B. W. C.; Bohndiek, S. E.; Gallagher, F. A.; Jarvis, L. B.; Smith, K. G. C.; Brindle, K. M. *Proc. Natl. Acad. Sci. U.S.A.* **2012**, *109*, 13374.

(76) Bohndiek, S. E.; Kettunen, M. I.; Hu, D.-E.; Kennedy, B. W. C.; Boren, J.; Gallagher, F. A.; Brindle, K. M. *J. Am. Chem. Soc.* **2011**, *133*, 11795.

(77) Keshari, K. R.; Kurhanewicz, J.; Bok, R.; Larson, P. E. Z.; Vigneron, D. B.; Wilson, D. M. *Proc. Natl. Acad. Sci. U.S.A.* **2011**, *108*, 18606.

(78) Keshari, K. R.; Sai, V.; Wang, Z. J.; VanBrocklin, H. F.; Kurhanewicz, J.; Wilson, D. M. *J. Nucl. Med.* **2013**, *54*, 922.

(79) Wiesinger, F.; Weidl, E.; Menzel, M. I.; Janich, M. A.; Khegai, O.; Glaser, S. J.; Haase, A.; Schwaiger, M.; Schulte, R. F. *Magn. Reson. Med.* **2012**, *68*, 8.

(80) Larson, P. E.; Hu, S.; Lustig, M.; Kerr, A. B.; Nelson, S. J.; Kurhanewicz, J.; Pauly, J. M.; Vigneron, D. B. *Magn. Reson. Med.* **2011**, *65*, 610.

(81) Cunningham, C. H.; Chen, A. P.; Lustig, M.; Hargreaves, B. A.; Lupo, J.; Xu, D.; Kurhanewicz, J.; Hurd, R. E.; Pauly, J. M.; Nelson, S. J.; Vigneron, D. B. *J. Magn. Reson.* **2008**, *193*, 139.

(82) Marusyk, A.; Almendro, V.; Polyak, K. *Nat. Rev. Cancer* **2012**, *12*, 323.